Rev. Adv. Mater. Sci. 33 (2013) 187-194

700MPa GRADE STEEL FOR HEAVY-DUTY TRUCK DEVELOPMENT AND CARRIAGE LIGHTWEIGHT DESIGN

Xiao Nan Wang[1], Qian Sun[2], Lin Xiu Du[3] and Hong Shuang Di[3]

[1]Shagang School of Iron and Steel, Soochow University, Suzhou, Jiangsu 215021, P. R. China
[2]AVIC Shenyang Aircraft Corporation, Shenyang, Liaoning 110034, P. R. China
[3]The State Key Laboratory of Rolling and Automation of Northeastern University, Shenyang, Liaoning 110819, P. R. China

Received: October 17, 2011

Abstract. In order to realize the weight reduction of the carriage of heavy-duty truck, the 700 MPa hot-rolled high-strength C-Mn steel plate was successfully developed on 1750 mm hot-strip mills to replace the Q345 steel plate which was originally used for carriage. The microstructure of the plate was composed of fine-grained ferrite, carbides distributed along the ferrite grain boundaries, a little pearlite with 40~50 nm lamellar spacing and a mount of bainite. The yield and tensile strengths of the plate were about 680 MPa and 740 MPa, respectively. The value of n, r_m and hole expansion rate (λ) were 0.12, 0.8, and 60%, respectively. The plate has great low temperature impact toughness and weldability. The strengthening mechanisms of the plate were mainly governed by fine-grained strengthening and (Ti,Nb)C nano-precipitates strengthening. If the carriage of heavy-duty truck was constructed by new plate, the weight could reduce 20% due to the thickness reduction. For further reduction of the weight of the carriage, the optimization design was carried out by finite element method. Then, the weight of the carriage could be reduced 12%.

1. INTRODUCTION

Heavy-duty truck has a big loadage, high transportation efficiency and good economy. Heavy-duty truck plays more important roles on large engineering, professional transport, container transport of wharf, and cross-border transportation [1-3]. Traditionally, the steel used in truck carriage was Q345. However, it has many problems such as fatigue fracture, expansion of carriage and bad impact resistance. At present, the chemical elements of Mo, Cr, and V were added in the high strength steel of 700 MPa during the production to obtain excellent properties. In the respect of control rolling, the thermo mechanical control process (TMCP) or the process combined TMCP with temper was adopted, and the cost became higher and more complicated [4-7]. For the lightweight design of automobile, materials substitution and structural optimization by CAE were disconnection [8,9]. Therefore, the maximum weight loss ratio has not be obtained, which limited the popularization and application of high strength steel.

Based on the lightweight design for the carriage of heavy-duty truck, the substitution material and structural optimization of carriage were studied in this literature. First, the 700 MPa hot-rolled high-strength C-Mn steel plate was successfully developed on 1750 mm hot-strip mills to replace the Q345. The micro-alloying elements Nb and Ti were used in the new material, and the microstructure, strengthening mechanisms and mechanical properties were studied. Second, before and after lightweight design, the static structural strength and rigidity of carriage were checked by finite element method. Finally, the carriage structure was optimized by modifying the finite element model.

Corresponding author: Lin Xiu Du, e-mail: wxn@suda.edu.cn

Table 1. Chemical compositions of carriage plate (wt.%).

C	Si	Mn	P	S	Al	Nb	Ti
≤0.12	≤0.3	≤2.2	≤0.015	≤0.010	≤0.06	≤0.08	≤0.14

Table 2. Basic program of numerical simulation study.

Case No.	BP thickness /mm	SP thickness /mm	MLG thickness /mm	SSG	other	Static load /t
ABC	867	644	877	866	No change	50

Remarks: Bottom plate-BP; Side plate-SP; main longitudinal girder -MLG; Side stiffener group- SSG

2. MATERIALS AND METHODS

2.1. Materials

Considering the actual production conditions and the production cost of carriage plate, the chemical compositions design should be low-carbon and high-titanium, as shown in Table 1. The smelting process was as follows: mixer furnace → hot metal pretreatment → LF refining furnace → continuous casting.

2.2. Methods

Metallographic specimens were polished and etched with 4% nital before examed by *LEICA-DMIRM* light microscopy (OM) and *FEI Quanta 600* scanning electron microscopy (SEM). *FEI Tecnai G² F20* transmission electron microscopy (TEM) was carried out on thin foils and carbon extraction replicas. Tensile test was performed by the *WDW*-300 tensile testing machine. Low temperature impact toughness was conducted by the *INSTRON* 9250 drop hammer impact test machine with "V"-type notched specimen (55 mm×10 mm×5 mm). Hole expanding performance was obtained by the stretch flangeability of the important parameters. Hole expanding test was based on the standard (GB/T 15825.4-2008) by the test machine *BCS* universal metal sheet forming. The sample was 100 mm×100 mm×2.5 mm plate with F16.5 mm hole prefabricated in the middle. Then, the hole was pressed by a circular vertex punch until crack. Based on "**equal strength matched**", the homemade *JM-100C* wire with the tensile strength of 745 MPa was used. The thickness, blunt edge and group space of welding sample was 8, 2, and 1.6 mm, respectively.

Table 2 shows the basic program of the numerical simulation. Case A was the on-site practical loading program, case B was the optimization solution progress provided by manufactures, and case C was the optimization program proposed by authors. SOLID 92 element was used as the geometric model. The model was composed of 210,000 elements. The displacement constraints in Y direction were applied on the longitudinal beam of sub-frame. The pressure was applied by sand on the car side which was calculated by the Rankine's earth pressure theory. The total earth pressure of the unit length of the car was calculated by the area of the triangle, the equation was shown in Eq. 1.

$$E_a = \left(\rho H^2 K_0\right)/2, \quad (1)$$

where ρ is the sand density (1850 kg/m^3), K_0 is the static pressure coefficient of soil, and E_a is action away from the car bottom about H/3 length which through the triangle centroid on the level direction [10].

3. RESULTS AND DISCUSSIONS

3.1. Microstructure

3.1.1. OM and SEM

The microstructure constituent of carriage plate was ferrite with boundary precipitation of fine carbides and a certain amount of pearlite and bainite. The ferrite grain size was in the range of 6~7 mm obtained by the secant method and a uniform size as shown in Fig. 1a. Fine-grained ferrite and the carbides in the grain boundary were distinct in the SEM image (Fig. 1b).

3.1.2. TEM

The fine microstructure of carriage plate was observed by TEM. There were equiaxial and non-equiaxial ferrite (Fig. 2a), with banded carbides of intergranular precipitation (Fig. 2b). Fig. 2c shows

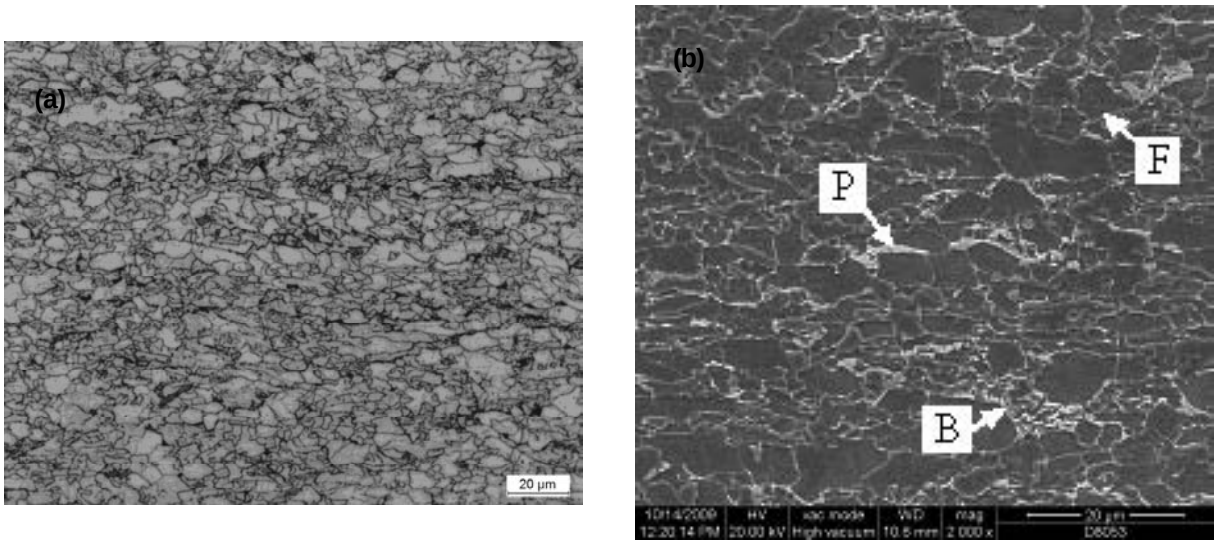

Fig. 1. Microstructures of carriage plate: (a) OM, (b) SEM.

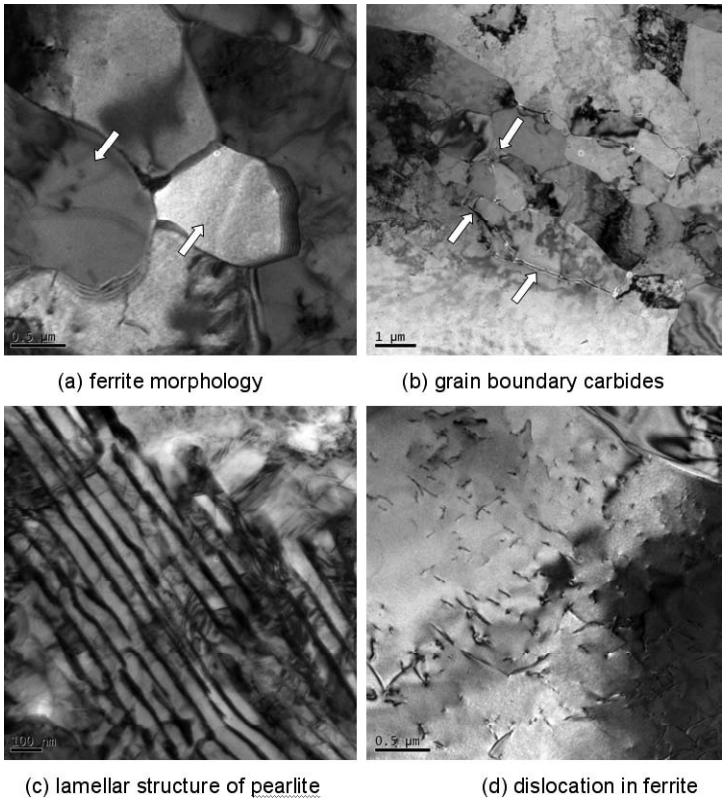

Fig. 2. TEM images of specimens: (a) ferrite morphology, (b) grain boundary carbides, (c) lamellar structure of pearlite, (d) dislocation in ferrite.

the pearlite organization. The interlamellar spacing was in the range of 40~50 nm. Temperature is one of the important factors which influence the pearlite interlamellar spacing. The pearlite interlamellar spacing will minish when the cooling rate is increased or the transition temperature of austenite is reduced. This organization has a certain impact on the fatigue properties of steel according to the references which will be further studied by fatigue test [11]. Fig. 2d shows the dislocation of ferrite with low dislocation density indicating that the contribution of dislocation strengthening was relatively weak.

3.2. Mechanical property

Yield strength of about 680 MPa, tensile strength of about 750 MPa, yield ration of 0.9 which resulting in good elongation. Strain hardening index n, the plastic strain ratio r_m were 0.12 and 0.82, respec-

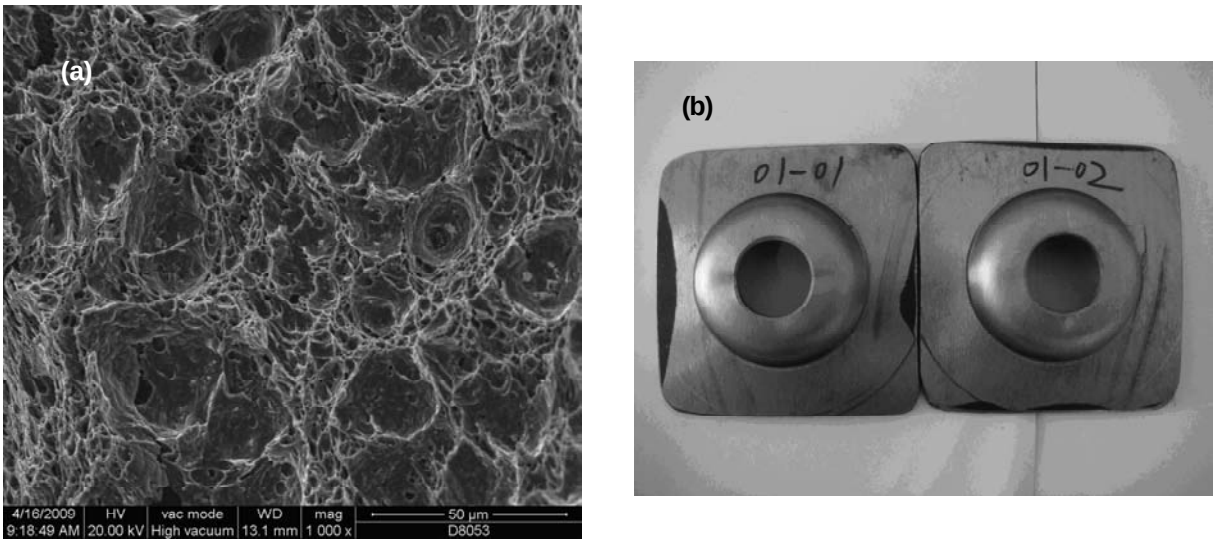

Fig. 3. SEM image of fracture and physical graph of hole expanding test: (a) SEM image of impact fracture, (b) physical graph of hole expanding test.

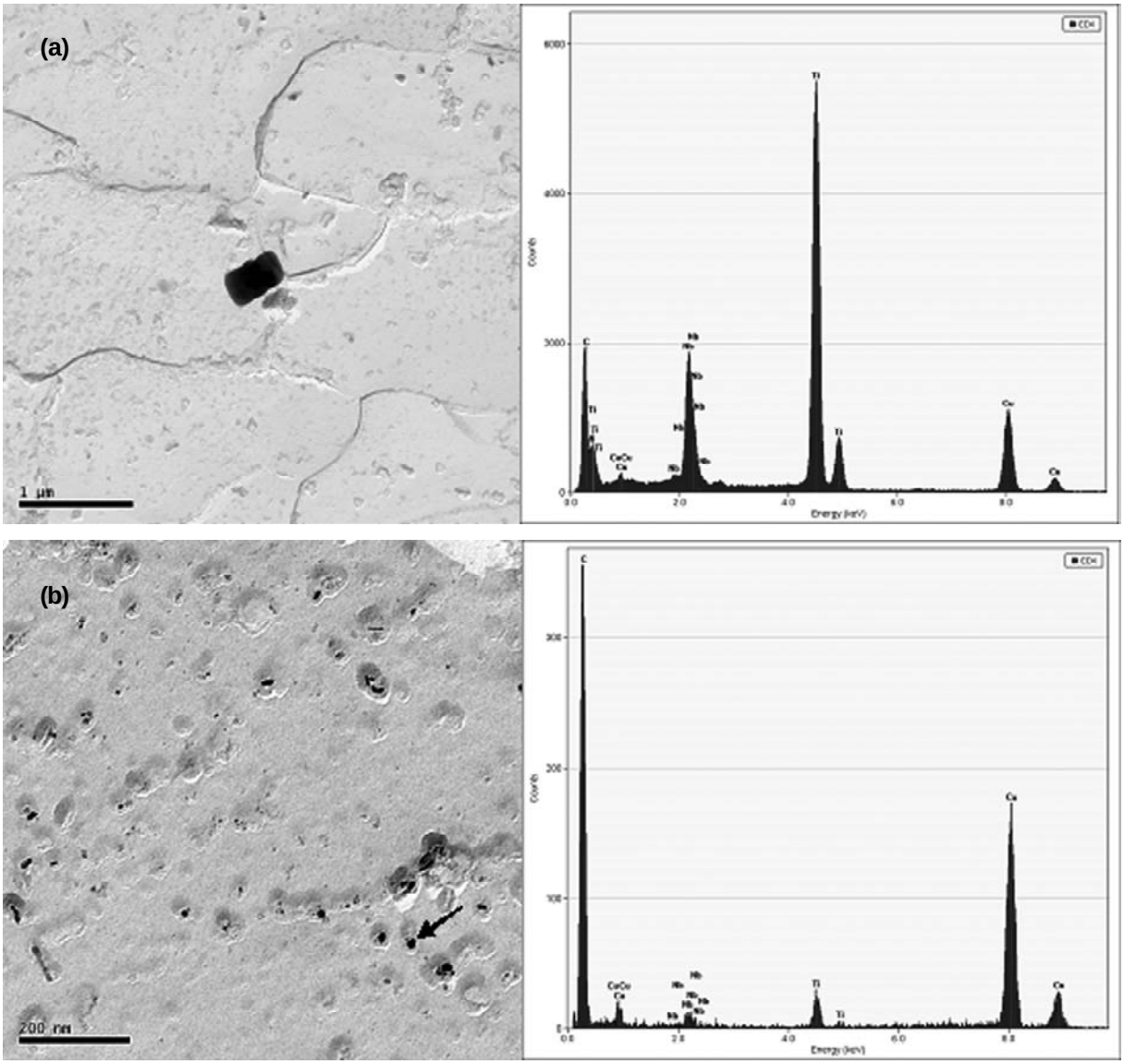

Fig. 4. Morphology of precipitates and their compositions: (a) large size precipitation (Ti,Nb)CN, (b) nanometer precipitates (Ti,Nb)C.

tively, which lead to good work-hardening ability and plastic deformation capacity. The impact energy at -70 °C was 75 J. Fig 3a shows the fracture morphology. It was ductile fracture. Hole expanding rate was 60%. Fig. 3b is the hole expanding test physical graph. Welding basic process was listed as follows: welding voltage 21~22 V, welding current of 210~220 A, shielding gas for the 100% CO_2, flow rate 20 L/min, semi-automatic welding using manual methods. After welding to avoid arcing segment and harvested arc segment to take tensile specimen, fracture location in the heat-affected zone is at the side of the weld bond, and the fracture strength was basically the same as the tensile strength of base material.

3.3. Nanometer precipitates

In Fig. 4a, the shape of precipitate is rectangular with a few hundred nanometers in size, and high content of Ti in precipitate known by energy dispersive X-ray detector (EDX) analysis. Therefore, the rectangular precipitates of large size are mainly TiN formed in liquid state or during steel processing in the solid state. It can be seen from Fig. 4b, the small size of precipitates was round or oval shape, and the size mostly concentrated in 10~20 nm, and even there is a certain amount of particles less than 10 nm. EDX composition analysis shows that less content of N in precipitates. As the N content in the carriage plate is very low (below 50 ppm), the majority of N in the form of TiN precipitates.

When the slab heated to rolling temperature, most of the Nb dissolution, while the TiN still in a stable condition for its high solution temperature (1300 °C). As the rolling process proceeded and the temperature of slab gradually decreased, Nb-containing particles to form around the nuclear center as TiN formed before and re-precipitation attached to it surface. Since the lattice types and lattice constants of Nb or Ti-C compounds, N compounds and the C,N compounds are nearly the same, with all NaCl-type face-centered cubic and lattice constant of between 4~45 nm, these compounds can be dissolved easily to form the (Nb,Ti)C. According to empirical Eq. (2), the steel yield strength equal to the amount of pure iron strength, solution strengthening, fine grain strengthening capacity and precipitation strengthening capacity.

$$\sigma = 53.9 + 32.34[\%\mathrm{Mn}] + 83.16[\%\mathrm{Si}] + 254.2[\%\mathrm{N}] + 17.4022d^{1/2}. \quad (2)$$

Using the formula to calculate the fundamental strength, where [%Mn], [%Si] and [%N] were solid solution of Mn, Si and N respectively. The element of N is related to micro-alloying elements form a nitride, so [%N] is zero. *d* for the ferrite grain size, calculation unit is mm [6]. According to the chemical composition and ferrite grain size of the carriage plate, the fundamental strength of carriage plate is calculated as 323 MPa. It is inferred from Fig. 3d that the dislocation strengthening of car plate steel is not obvious. Therefore, Precipitation strengthening can gave contribution of ~300 MPa. The strengthening mechanisms of carriage plate are mainly fine-grain strengthening and precipitation strengthening.

3.4. Numerical simulation results and analysis

3.4.1. Analysis of carriage equivalent stress values (SEQV)

Fig. 5 shows the distribution contour of equivalent stress of carriage with 50t static load. The maximum values of equivalent stresses was in main longitudinal girder (MLG). Comparing case A and B, the SEQV values of MLG was increased almost 31%, and the SEQV value of case B reached to yielded strength (680 MPa). Therefore, the case B did not meet the requirement of structural strength. Comparing case A and C, the maximum value of SEQV increased almost 13%. However, in case C, the maximum value of SEQV was 590 MPa, and 90 MPa was strength margin. The safety strength margin reached to 1-590/680=13%. Case C was adopted when the thickness of bottom plate reduction was used to optimum design. Case B was not discussed in detail.

3.4.2. Analysis of carriage total elastic displacement

Fig. 6 shows the distribution contour of elastic displacement of carriage with 50 t static load. The maximum and minimum elastic displacements appeared in the upper and middle section of the side and middle section of the carriage floor. The maximum elastic displacements of different sections were 10.333 mm and 14.178 mm, respectively. The minimum value was 0 (longitudinal beam on sub-frame is fixed). With 50 t static load, the total elastic displacement calculated by case A is smaller than case C. The stiffness of isotropic materials depends on its elastic modulus *E*, shear modulus *G* where the shear modulus *G* can be calculated using the following Eq. 3:

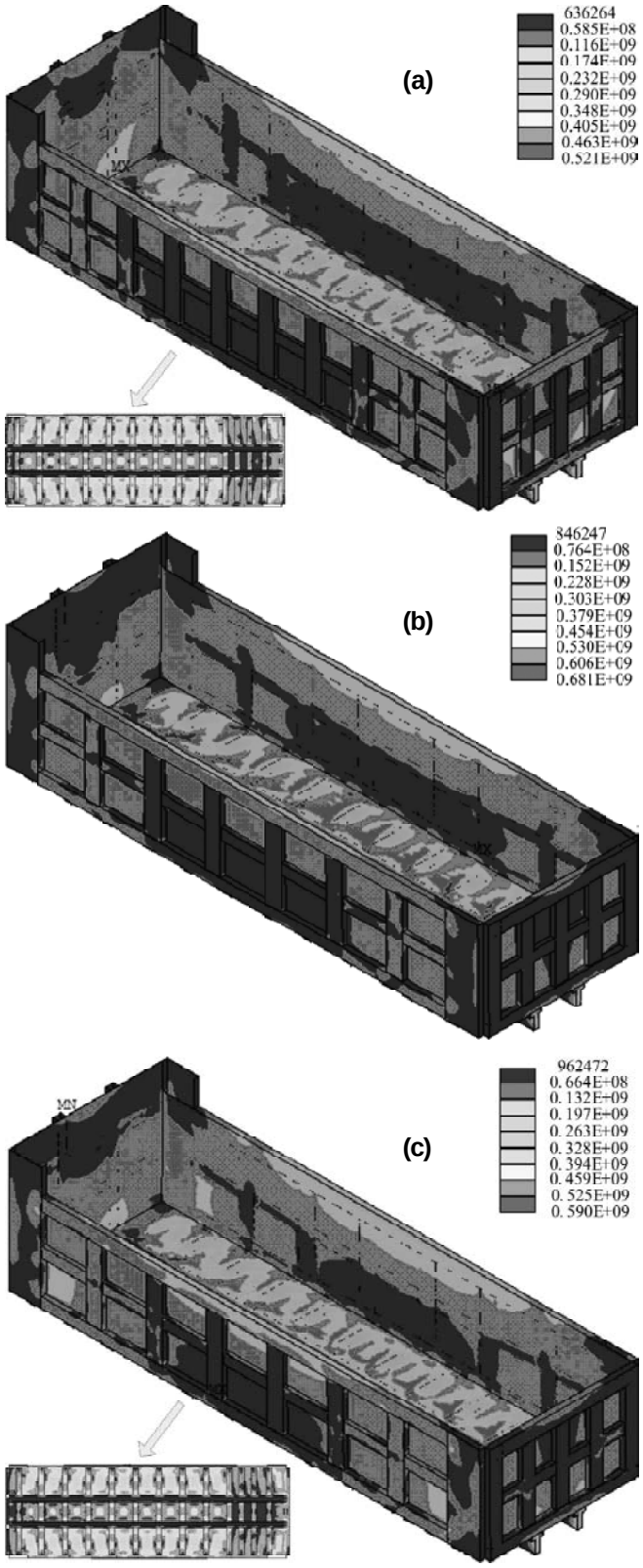

Fig. 5. Distribution maps of equivalent stress of carriages: (a) case A, (b) case B, (c) case C.

$$G = E / 2(1+\gamma), \quad (3)$$

where g is Poisson's ratio. The stiffness of structure depends on the stiffness of the material, external force, geometry, boundary conditions and other factors. A numerical simulation case and C case have the same elastic modulus, boundary conditions and external force, but the geometric shape was different with the thinner carriage plate used in case C. The total elastic displacement of carriage plate

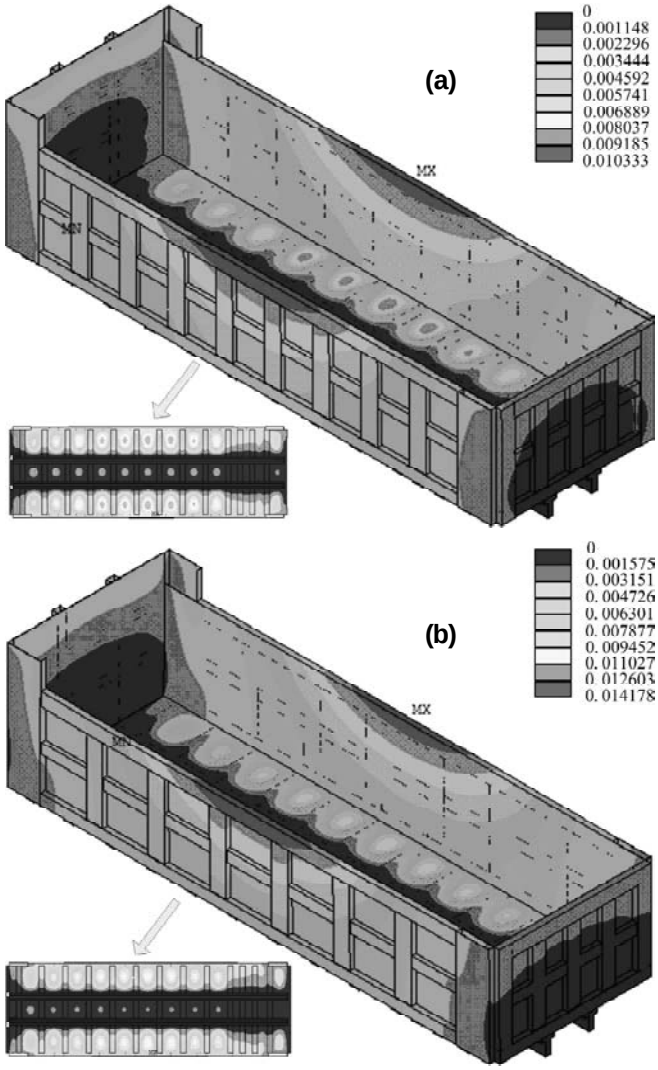

Fig. 6. Distribution maps general of elastic displacement of carriages: (a) case A, (b) case C.

in C case increased and the static structural stiffness decreased. The remained strength (90 MPa) can meet the structural weight loss goal. The total volumes calculated by case A and C are 4548 kg and 3975 kg, respectively. The weight loss ratio was 12.6%, which realized the purpose of optimization design.

4. CONCLUSIONS

Through the combination of product development and the finite element simulation of 700 MPa hot-rolled high-strength C-Mn steel plate, lightweight design and structure optimization are done for heavy-duty truck to achieve the purpose of lightweight cars. The microstructure of carriage plate is fine-grained ferrite and small carbides on grain boundary, also there is a small amount of pearlite which has lamellar spacing of 40~50 nm and some banitie. The mechanisms of strengthen are mainly caused by fine-grain strengthening and precipitation strengthening with nano-precipitates of (Nb,Ti)C, and precipitation strengthening can gave contribution of ~300 MPa. The car plate has good low temperature impact toughness, weld ability and stretch flangeability, *etc*. If the carriage is constructed by using the new plate, the weight of it can be reduce about 20% due to the thickness reduction. The structure has been optimized designed by using FEM which produced a further 12% weight loss. A basis theory for further actual production and solving the “expansion of carriage” is provided.

ACKNOWLEDGEMENTS

This work was supported by the Special Program for Key Research of Chinese National Basic Research Program (2011CB606306-2) and the Fundamental Research Funds for the Central Universities (N090607003).

REFERENCES

[1] T. Huai, S.D. Shah, J. W. Miller, T. Younglove, D.J. Chernich and A. Ayala // *Atmos. Environ*. **40** (2006) 2333.
[2] C.J. Brodrick, T.E. Lipman, M. Farshchi, N.P. Lutsey, H.A. Dwyer, D. Sperling, S.William Gouse, D. Bruce Harris and F.G. King // *Transport. Res*. *D-TR. E.* **7** (2002) 303.
[3] D.H. Kim, M. Gautam and D. Gera // *Atmos. Environ*. **25** (2001) 5267.
[4] R.D.K. Misra, H. Nathani, J.E. Hartmann and F. Siciliano // *Mater. Sci. and Eng. A* **394** (2005) 339.
[5] N. Naki and M. Matthias // *ISIJ Int*. **45** (2005) 82.
[6] Y. Funakawa, T. Shiozaki, K. Tomita, T. Yamamoto and E. Maeda // *ISIJ Int.* **44** (2004) 1945.
[7] L.X. Du, D.S. Liu, X.H. Liu and G.D. Wang // *Mater. Mech. Eng.* **24** (2000) 8.
[8] L.S. Wang, P.K. Basu and J.P. Leiva // *Finite Elem. Anal. Des.* **40** (2004) 879.
[9] X.N. Wang, H.S. Di, B.J . Liang and L.X. Du // *J. Northeast. Univ. (Nat. Sci.)* **30** (2010) 60.
[10] Y.H. Xi and J.F. Chen, *Soil Mechanics and Foundation Engineering* (Tung chi university press, Shanghai, 2006).
[11] Z.C. Liu, *Material Changes in the Organizational Structure of Principe* (Metallurgy industry press, Beijing, 2006).